CARTILAGE
January-March 2022: 1–13
© The Author(s) 2022
DOI: 10.1177/19476035221085143
journals.sagepub.com/home/CAR
SAGE

Location-Specific Study of Young Rabbit Femoral Cartilage by Quantitative μMRI and Polarized Light Microscopy

Syeda Batool[1], Mouhamad Hammami[1], Hannah Mantebea[1], Farid Badar[1], and Yang Xia[1]

Abstract

Objective. Microscopic magnetic resonance imaging (μMRI) and polarized light microscopy (PLM) are used to characterize the structural variations at different anatomical locations of femoral cartilage in young rabbits (12-14 weeks old). *Design.* Four intact knees were imaged by μMRI at 86 μm resolution. Three small cartilage-bone specimens were harvested from each of 2 femoral medial condyles and imaged by quantitative μMRI (T2 anisotropy) at 9.75 μm resolution ($N = 6$). These specimens, as well as the other 2 intact femoral condyles, were used for histology and imaged by quantitative PLM (retardation and angle) at 0.25 μm to 4 μm resolutions. *Results.* Quantitative MRI relaxation data and PLM fibril data revealed collaboratively distinct topographical variations in both cartilage thickness and its collagen organization in the juvenile joint. Cartilage characteristics from the central location have a 3-zone arcade-like fibril structure and a distinct magic angle effect, commonly seen in mature articular cartilage, while cartilage at the anterior location lacks these characteristics. Overall, the lowest retardation values and isotropic T2 values have been found in the distal femur (trochlear ridge), with predominant parallel fibers with respect to the articular surface. Central cartilage is the thickest (~550 μm), approximately twice as thick as the anterior and posterior locations. *Conclusion.* Distinctly different characteristics of tissue properties were found in cartilage at different topographical locations on femoral condyle in rabbits. Knowledge of location-specific structural differences in the collagen network over the joint surface can improve the understanding of local mechanobiology and provide insights to tissue engineering and degradation repairs.

Keywords

collagen network, articular cartilage, μMRI T2 anisotropy, polarized light microscopy angle and retardation, topographic variation

Introduction

Articular cartilage (AC) is a thin layer of protective and shock-absorbing tissue that distributes loads effectively over a joint surface. AC has very limited healing potential and can develop degenerative changes due to aging, excessive usage, and trauma, which all eventually clinically lead to osteoarthritis and other joint diseases.[1,2] Aging has been considered a primary risk factor of osteoarthritis, which may start with biologically and mechanically compromised AC, and subsequently results in tissue loss and bone deformation. As any joint has specific 3-dimensional (3D) shapes or contours and a unique set of biomechanical environments, any joint degradation at its early stages must have complex variations over joint surfaces, dependent upon the location of the initiation event.[3,4] A recent study[5] has reported age-related topographical variations in terms of cartilage thickness, biomechanical response, and subchondral bone measurements in rat knees after surgical destabilization of the medial meniscus. As bone and cartilage are interdependent structural components in any joint, the loading conditions during the aging process are speculated to modulate the structural and physiological responses of bone, as well as AC, which can be highly localized.[6]

AC contains living cells (chondrocytes) embedded in an extracellular matrix (ECM). ECM consists mainly of proteoglycans (PG), type II collagen fibrils, and water (65%-80%). The architecture of ECM in adult AC is dominated by its

[1]Department of Physics, Center for Biomedical Research, Oakland University, Rochester, MI, USA

Corresponding Author:
Yang Xia, Department of Physics, Center for Biomedical Research, Oakland University, 244 Meadow Brook Road, Rochester, MI 48309, USA.
Email: xia@oakland.edu

collagen network, which possesses a 3-zone arcade-like fibril structure.[7] Starting from the top articular surface, mature AC can be subdivided into 3 zones based on this arcade-like structure, beginning with the superficial zone (SZ) where fibers run in parallel with the surface, continuing to the transitional zone (TZ) where fibers run randomly without a predominant orientation, and ending with the radial zone (RZ) where fibers are oriented mainly perpendicular to the surface. In comparison, neonatal cartilage is known to lack this arcade-like zonal structure and appears more homogeneous and isotropic with a higher matrix to cell ratio. Although the mechanisms involving the remodeling of mostly isotropic neonatal cartilage into the arcade-like structure in mature cartilage is still not clear, there is strong evidence of significant structural adaptations with age and exercise.[8-10] Better understanding of the age-related changes in cartilage morphology should provide new insights toward the progression of disease in patients at different age groups and the design of more effective ways to repair degradative tissue.

In this study, we use quantitative protocols in microscopic magnetic resonance imaging (μMRI) and polarized light microscopy (PLM) to assess the structural variations in young (skeletally immature) cartilage at different locations of femoral condyle in rabbits. In μMRI studies of cartilage, T2 anisotropy is known to be sensitive to the organizational architecture of the collagen fibrils in AC, which gives rise to the well-known laminar appearance in T2-weighted MRI images.[11,12] In PLM, the birefringence properties of ECM in cartilage can be quantitatively examined by the retardation and angle measurements, which correspond to fibril organization and fibril orientation respectively.[13-15] There exists a number of well-established in situ correlations between T2 anisotropic properties and the birefringence properties in cartilage and other connective tissues.[13] This study aims to better understand the structural specifics in skeletally immature tissue in the rabbit model, related to its potential in the use of osteoarthritis studies, and the remodeling of the collagen fibril network during growth and maturation at different anatomical locations over the same joint surface.

Material and Methods

MRI of Intact Joint

Four knee joints from 12- to 14-week-old healthy rabbits (White New Zealand, male) were obtained from a nearby higher education institution. The animals were sacrificed for an unrelated biomedical study, which was approved by the relevant institutional review committees (PROTO202000161). The animals were frozen immediately at –80 °C after necropsy and thawed at 4 °C before specimen harvesting. Each intact joint was placed in a glass tube with a cotton swab soaked with physiological saline to avoid dehydration and imaged at room temperature using a Bruker AVANCE IIIHD NMR spectrometer equipped with a 7 Tesla/89 mm magnet and 25 mm rf resonator (Bruker, Ettlingen, Germany).

All 4 intact knees were imaged in sagittal and coronal views using the standard multi-slice multi-echo sequence, where each imaging experiment had 8-10 slices and each slice had 6-8 intensity images. Each slice had a thickness of 0.8 mm with a gap of 1 mm between any two neighboring slices. The imaging TE was 8.23 ms, and the TR was 3 s. The field of view (FOV) was 22×22 mm^2 and the 2-dimensional (2D) acquisition matrix was 256×128, which was later reconstructed to 256×256, resulting in a pixel size of 86 μm.

μMRI of Cartilage-Bone Specimens

After imaging the intact joints, 2 knees were opened (**Fig. 1A**) to harvest the cartilage-bone specimens from the femoral medial condyles. Each condyle was cut into 3 slices (**Fig. 1E**), which were ~1.6-1.8 mm in thickness. Three individual cartilage-bone specimens were harvested from 3 different locations on the same (middle) condyle slice (**Fig. 1F**), which were named anterior (A), central (C), and posterior (P), respectively. Each cartilage-bone specimen was rectangular, approximately $1.8 \times 2 \times 2.5$ mm^3 in size, and still had a full thickness of AC attached to the underlying bone. All cartilage-bone specimens were equilibrated in saline with 154 mM protease inhibitors. The total number of cartilage-bone specimens for μMRI was 6 (with 2 for each location).

Each of the cartilage-bone specimens was imaged independently 5 times using the identical imaging parameters, with the exception of the physical orientations of the specimen with respect to the external magnetic field B0, ranging from 0° to 125° (where 0° is defined as the normal axis of cartilage surface being in parallel with B0), with the use of a homebuilt rotating device.[16] A magnetization-prepared 2D spin-echo sequence was used for the quantitative T2 imaging of all cartilage-bone specimens, with TR of 2 s, TE of 6.47 ms, and the slice thickness of 0.8 mm. The location of the slices throughout each series of imaging experiments was identified to be the same during the project. The 2D matrix was 256×128, which was reconstructed into 256×256; the FOV was 2.5×2.5 mm^2, resulting in a pixel size of 9.75 μm for all cartilage specimens.[12,17] The TEs of the leading contrast segment (TEc) had 4 increments: 2, 16, 22, and 46 ms for the central (C) and posterior (P) specimens and 2, 16, 46, and 60 ms for the anterior (A) specimens.

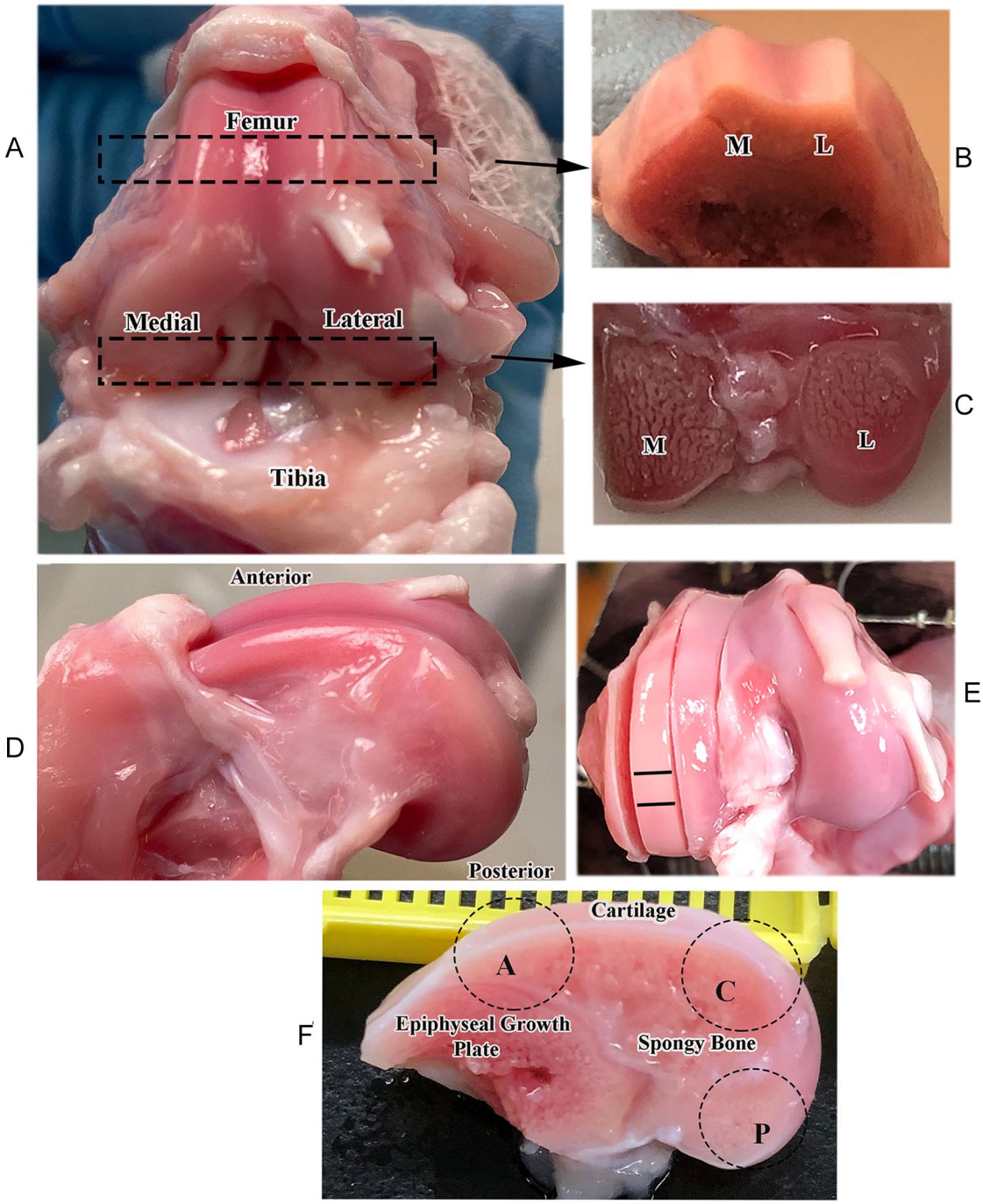

Figure 1. (**A**) The right knee of a 3-month-old rabbit, exposing both medial and lateral condyles of a femur. (**B**) The cross-sectional slice at the patellofemoral location of femur covering both medial and lateral condyles before its split. (**C**) The cross-sectional slice at the tibiofemoral location of femur covering both condyles. (**D**) Side view of an un-sectioned femur medial condyle. (**E**) The medial condyle is sectioned into three ~1.6- to 1.8-mm-thick cartilage-bone slices longitudinally. The central slice, which runs up to the unsplit part of femur, is further cut into small rectangular cartilage-bone specimens (~1.8 × 2 × 2.5 mm^3) for high-resolution μMRI and PLM. Two thin lines mark the location of the central specimen on the central slice. (**F**) Side view of a central slice of medial condyle with 3 designated locations (A, C, and P) for μMRI specimens. μMRI = microscopic magnetic resonance imaging; PLM = polarized light microscopy.

PLM Specimens and Protocol

All 6 cartilage-bone specimens after the noninvasive μMRI were processed for histology. In addition, 2 remaining intact joints were processed for whole-joint histology, where the full-length and width slabs (4-5 mm thick) were cut in transverse planes (across tibiofemoral and patellofemoral regions, as in **Fig. 1B** and **1C**) and along the middle of the medial condyle (including all 3 μMRI sites, as in **Fig. 1F**). All histology specimens were fixated in 10% neutral-buffered formalin overnight at room temperature. All fixated specimens were sent to a histology service (Yale Pathology Tissue Services, CT), which cut the specimens at specified locations into 6-μm thin sections using the paraffin embedding method. Three sections from each cartilage-bone specimen (the μMRI samples) and 3 sections from each longitudinal and lateral slab were imaged using a digital PLM system (Leica, Wetzlar, Germany and Cambridge Research & Instrumentation, Hopkinton, MA). Each imaging acquisition in the digital PLM system generated 2 quantitative images: the optical retardation (in unit of nm) and the angular orientation (in unit of degrees). The angle image represents the voxel-averaged orientations of the collagen fibrils, whereas the retardation image represents the voxel-averaged organization of the collagen fibrils in tissue.[13]

Each cartilage-bone specimen (A, C, and P) had at least 3 full-thickness histological sections, which were imaged individually at the identical orientation under 10x and 40x objectives. This yielded a pixel size of 1 μm and 0.25 μm, respectively. The 10x images were used for quantitative retardation and azimuthal profiles, and the 40x images were used to observe the territorial matrix surrounding the individual chondrocytes at different depths. Histological sections of the intact femoral condyles were imaged under 2.5x and 5x objectives, which yielded pixel sizes of 4 μm and 2 μm, respectively. These low-resolution optical images were used to study the heterogeneity of collagen fibril organization across the intact femoral condyles in orthogonal directions.

Image and Data Analysis

Quantitative maps of T2 relaxation were calculated by a single exponential fitting of the data on a pixel-by-pixel basis for all specimens. Each cartilage-bone specimen was imaged in μMRI 5 times at 5 different orientations, with respect to B0, which resulted in 20 independent proton images and 5 calculated T2 maps for each specimen. On each quantitative 2D T2 image, 1 rectangular region of interest (ROI), with 15 parallel neighboring columns, was selected manually and averaged into one 1-dimensional (1D) depth-dependent T2 profile, which enabled the observation of the depth-dependent T2 anisotropy in the tissue and the comparison among profiles from different imaging experiments. As the column-averaging occurred perpendicular to the tissue depth, the pixel resolution in the T2 profiles was still 9.75 μm along the tissue depth. The width and location of ROI were the same for all independent imaging experiments of each sample, with the use of the image analysis software ImageJ. All 2D images and 1D profiles, where each came from 1 independent imaging experiment, used the identical scaling and settings without any additional adjustment.

On each quantitative PLM image of cartilage specimens obtained at 10x objective, 146 parallel neighboring columns, which would have approximately the same width as the ROI thickness in μMRI, were averaged to produce 1 pair of 1D quantitative retardation and angle profiles across all tissue zones. The 40x images enabled the visualization of the shape and orientations of chondrocytes, with respect to the surrounding territorial and interterritorial matrix at different depths (histological zones) among all histological sections from 3 locations. The post-acquisition analysis used a public domain software ImageJ (NIH) and a commercial software KaleidaGraph (v4, Synergy Software, Reading, PA).

Results

MRI of the Intact Knee Joint

Before opening the knee joints, the intact knees were imaged by μMRI at the pixel resolution of 86 μm. **Figure 2** shows the sagittal and coronal views of T2-weighted intensity images, respectively, together with their respective quantitative T2 images. The epiphyseal cartilage (growth plate) appears brighter and homogeneous in intensity; in contrast, signal variations can be seen over the thickness of AC, especially in femur, even at the low 86-μm resolution. The appearance of AC in T2-weighted MRI images was highly sensitive to its orientation with respect to the external magnetic field B0 (vertically up). Because of its curved articular surface, the femoral condyle provides a convenient model to study the orientation effect of cartilage T2 relaxation with respect to B0 (i.e., the magic angle effect), as long as the quality of cartilage is the same at every location. If T2-sensitive structural variations exist as expected in juvenile joint during development, the interpretation of imaging results needs additional considerations. In our imaging results, among the 3 topographical locations on the central medial femur, the central location (C) was at about the magic angle (~54.74°) to B0 (sagittal view), where the influence of the dipolar interaction to the spin-spin relaxation was minimized; consequently, the cartilage in the central region appeared thicker than at the 2 other locations, anterior (A) and posterior (P). Away from the magic angle location, the femoral cartilage appeared bilaminar, with a high intensity surface layer and a low-intensity deep layer.

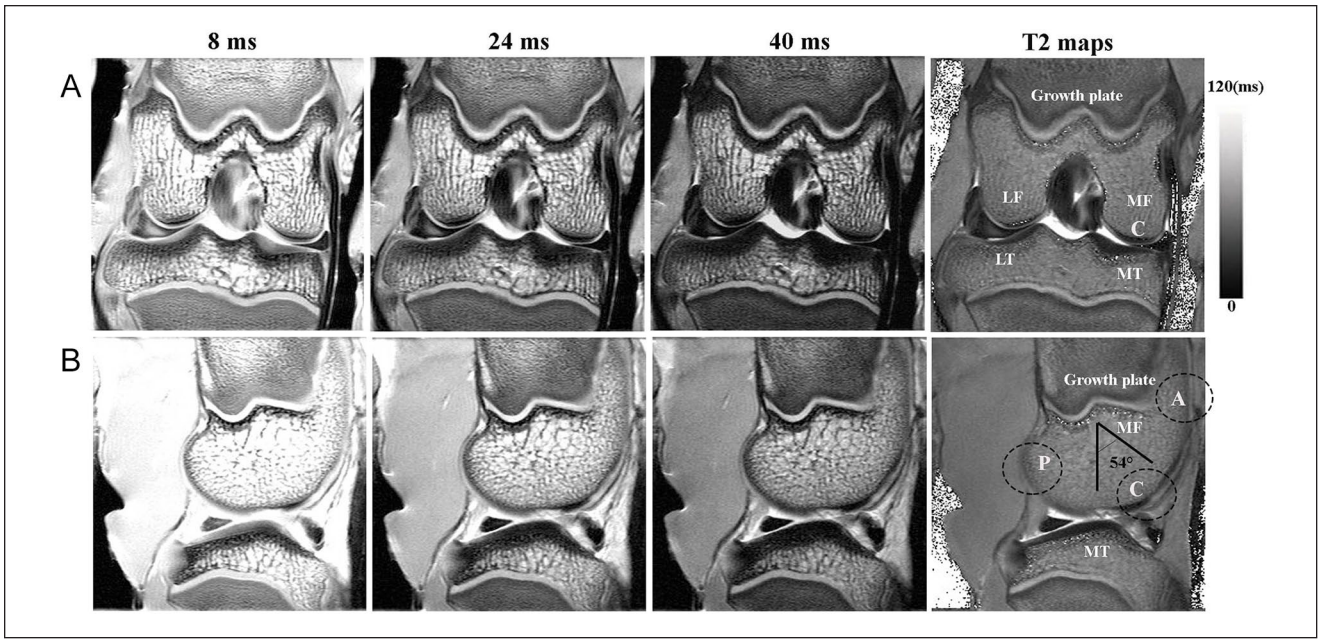

Figure 2. (**A**) Coronal T2-weighted intensity images and corresponding T2 map, and (**B**) sagittal T2-weighted intensity images and its corresponding T2 map. Each set of T2-weighted intensity images had 10 individual images, each at a different echo time. These intensity images were used to calculate 1 quantitative T2 image. Three designated locations, labeled as central (C), posterior (P), and anterior (A) on the medial condyle, were selected for μMRI T2 experiments. All images are displayed using the same up/low limits on a gray scale. μMRI = microscopic magnetic resonance imaging; LF = lateral femur; LT = lateral tibia; MF = medial femur; MT = medial tibia.

Due to the pixel size, signal variations for thinner regions (A and P) can be influenced by the volume averaging effect in imaging.

PLM Images of the Intact Femur Joint at 4 μm Resolution

Figure 3 displays the quantitative retardation images of the whole joint by PLM, at the 3 cross-sectional surfaces shown previously in **Figure 1B, 1C**, and **1F**. (Multiple retardation images were acquired individually in PLM and pieced together without any additional intensity adjustment.) **Figure 3A** is the retardation image of a longitudinal section of a femoral medial condyle at 4 μm pixel resolution (from the tissue block as in **Fig. 1F**), which showed that femoral cartilage was thinner at peripheries and thicker in the central region. Three topographical variations were determined from this image. First, the central cartilage was about 600 μm in thickness, twice the thicknesses when compared with the anterior and posterior cartilage (~300 μm). This PLM observation is consistent with the MRI results of knee joints in **Figure 2**. Second, the values of retardation were the lowest at the anterior site and highest at the central site, where most of the deep central cartilage had high retardation (i.e., high coherence in fibril organization) and most of the anterior site had very low retardation (i.e., low coherence in fibril organization). Finally, the lowest values of retardation at any topographical location occurred consistently at approximately 35 μm to 40 μm below the articular surface, regardless of the total thickness of the cartilage at this location.

Figure 3B and **3C** show the retardation images of 2 cross sections taken transversely or orthogonally from the anterior (patellofemoral) location of the femur (which opposes the patellar cartilage) and the central (tibiofemoral) location of the femur (which opposes the tibial cartilage) as shown in **Figure 3A** (as well as shown previously in **Fig. 1B** and **1C**). Two observations can be made for these cross sections. First, there is little difference in cartilage thickness across most of these transverse/orthogonal sections (except at the peripheral edges). Second, the femoral cartilage (**Fig. 3B**) from the central cross section seemed to have more variations in the structural patterns across the tissue depth. For example, this occurred between the cartilage at the trochlear ridges (TRs) and the cartilage in the central trochlear groove (TG). For these reasons, 1 ROI was selected from the central location of the medial femoral head (shown in **Fig. 3C**), and 2 ROIs were selected from the anterior cartilage opposing the patellar cartilage (shown in **Fig. 3B**).

MRI of Site-Specific T2 Anisotropy Results

Figure 4 shows the T2 anisotropy results at the higher spatial resolution of 9.75 μm in μMRI from 3 specimens

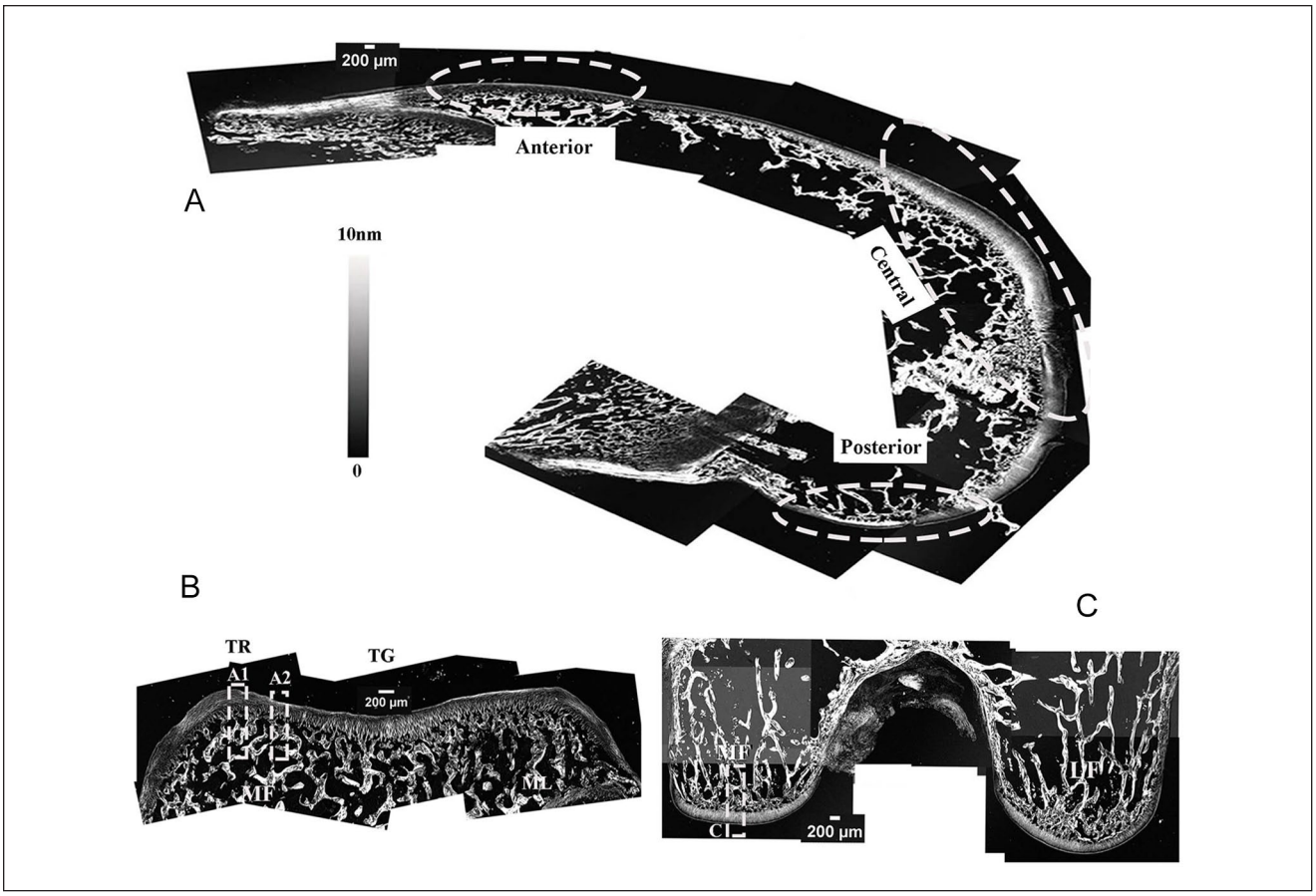

Figure 3. (**A**) The quantitative retardation images of the longitudinal slice from a femoral medial condyle (4 μm/pixel) are displayed with identical intensity limits (0-10 nm). Three white elliptical shapes show the locations where the small specimens were harvested for μMRI. (**B**) The retardation images (2 μm/pixel) from a tissue slice that harvested transversely to the slice in (**A**), approximately at the anterior location. (**C**) The retardation images (4 μm/pixel) from a tissue slice that harvested transversely to the slice in (**A**), approximately at the central location where the femur has 2 distinct medial and lateral condyles. The transverse planes on these slices are approximately at the same imaging planes as in μMRI. Three dashed rectangular boxes (A1, A2, and C) in (**B**) and (**C**) are the ROIs selected on the cartilage-bone specimens for quantitative imaging. μMRI = microscopic magnetic resonance imaging; ROIs = regions of interest; TR = trochlear ridge; TG = trochlear groove; MF = medial femoral; ML = medial lateral; LF = lateral femur.

acquired from the anterior, central, and posterior regions of femoral medial condyle, shown previously in **Figures 1F** and **3A**. (Note that each specimen was imaged 5 times between the orientations of 0° and 120°. As these images appeared similar visually, only 2 images for each location were shown in the figure. The most insightful information of T2 anisotropy among each set of 5 images can be obtained from the depth-dependent profiles in **Fig. 4**, which contain all orientations at all locations.) The images and anisotropy profiles of cartilage from the central (C) location have the familiar features that assemble the well-known T2 anisotropy under the influence of the dipolar interaction.[12,18] Based on the data at 55°, the cartilage thickness was ~500 μm at the central location. When the specimen was oriented at 0°, where the dipolar interaction is the strongest, most of the deep tissue had little signal in the spin-echo-based imaging sequences. This caused the truncation of the T2 (0°) profile to a depth of ~200 μm, beyond which the signal became too low to be reliably used to calculate T2 (the TE in the imaging sequence is 6.47 ms). Compared with the central cartilage, the posterior cartilage was about 50% more thin, at ~350 μm. T2 (0°) profile followed approximately the bell-shaped curve as seen in the central cartilage, but the peak was not as sharp and occurred deep in the percentage thickness. The rest of the T2 depth profiles did not strictly follow the T2 anisotropy as observed in the central cartilage. This implies that the overall orientational structure of the collagen fibers in the posterior cartilage might be slightly different than the central cartilage. But at large it followed the usual 3-zone structure as seen in mature cartilage. The anterior cartilage had the most curvatures and its T2 depth profiles had the most complicated variations. Two

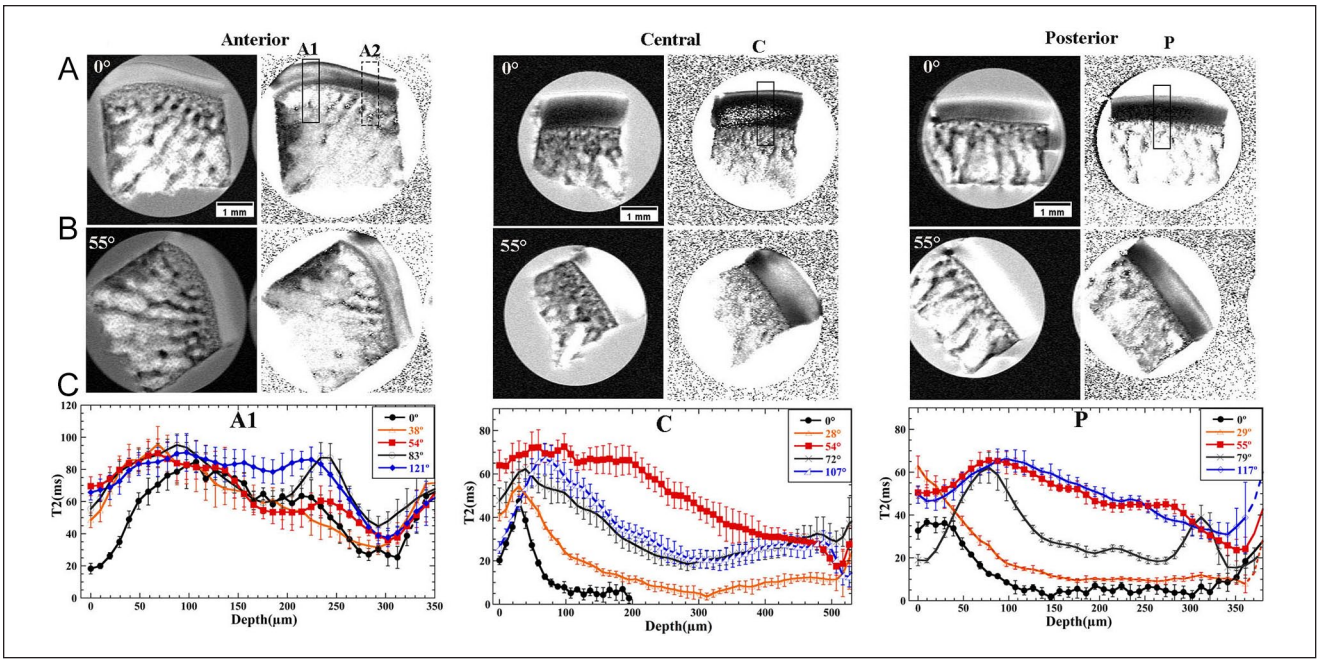

Figure 4. Two-dimensional μMRI intensity images (left) and corresponding T2 images (right) of 3 small cartilage-bone specimens harvested from 3 designated locations on the slice of femoral medial condyle, imaged at 9.75 μm/pixel at (**A**) 0° and (**B**) 55° with respect to the external magnetic field (B0), which was vertically up in the images. Each of the 3 samples was imaged under the identical parameters except for its orientations in B_0. As the anterior specimen had the most curved surface, 2 ROIs (A1 and A2) were selected, where A1 location is closer to the trochlear ridge (TR) and A2 is toward the trochlear groove (TG). (**C**) Quantitative T2 profiles from the cartilage in the ROIs (A1, C, and P), where the standard deviations of the averaged T2 data over the width of the ROI are represented by the vertical error bars. μMRI = microscopic magnetic resonance imaging; ROIs = regions of interest.

ROIs (A1 and A2) were selected for the anterior specimen, where A1 is located at the anatomical location of the TR and A2 is located in proximity of the TG. The T2 depth profiles from the A1 location lost all recognizable features as shown in the central cartilage, which implies that its collagen matrix did not have any of the usual 3-zone structure.

Quantitative PLM Images of Cartilage-Bone Specimens (10x Imaging)

Figure 5 shows the quantitative PLM results at 1 μm pixel resolution from the cartilage specimens at 3 topographical locations on the medial femur, whose μMRI data were presented in **Figure 4**. In the quantitative retardation images, the small black "holes" inside the AC are the locations where the cells and cell clusters used to reside (the particular histology procedure did not preserve the cellular details). In these angle images, blue and red indicated a 90° difference between the fibril orientations; the same 90° difference also existed between black and white, which had a 45° shift in the orientation to the blue and red combination.

Several features can be identified among the specimens obtained from 3 different anatomical locations of the joint. First, the PLM images and profiles for cartilage from the central location showed that the tissue had the arched 3-zone fibril architecture, where the surface fibers and the radial fibers had a 90° difference in their angular orientations (represented by blue and red, respectively, in the image). This observation agrees with the quantitative μMRI data discussed previously in **Figure 4**, and this agreement between the μMRI and PLM data is also consistent with the observations from many mature cartilage tissues from larger animals such as canines.[13] With this understanding, one can easily see that the collagen fibers in the posterior cartilage also have the arched 3-zone architecture, except that the tissue is thinner.

Second, as we have observed in the μMRI T2 anisotropy data (**Fig. 4C**), cartilage from the anterior location has the fibril architecture that is far from the arched 3-zone structure. This μMRI observation can be confirmed by the high-resolution PLM data in **Figure 5**. Comparing the 2D images between the anterior location and the central location, it is easy to recognize the continued variation of fibril structure even within the short length of the anterior cartilage block (~1.5 mm). As the orientations of the black oval-shaped cell void in the retardation images, which follows the local orientations of the collagen fibers in the territorial matrix of the tissue, one recognizes the transition from the right end

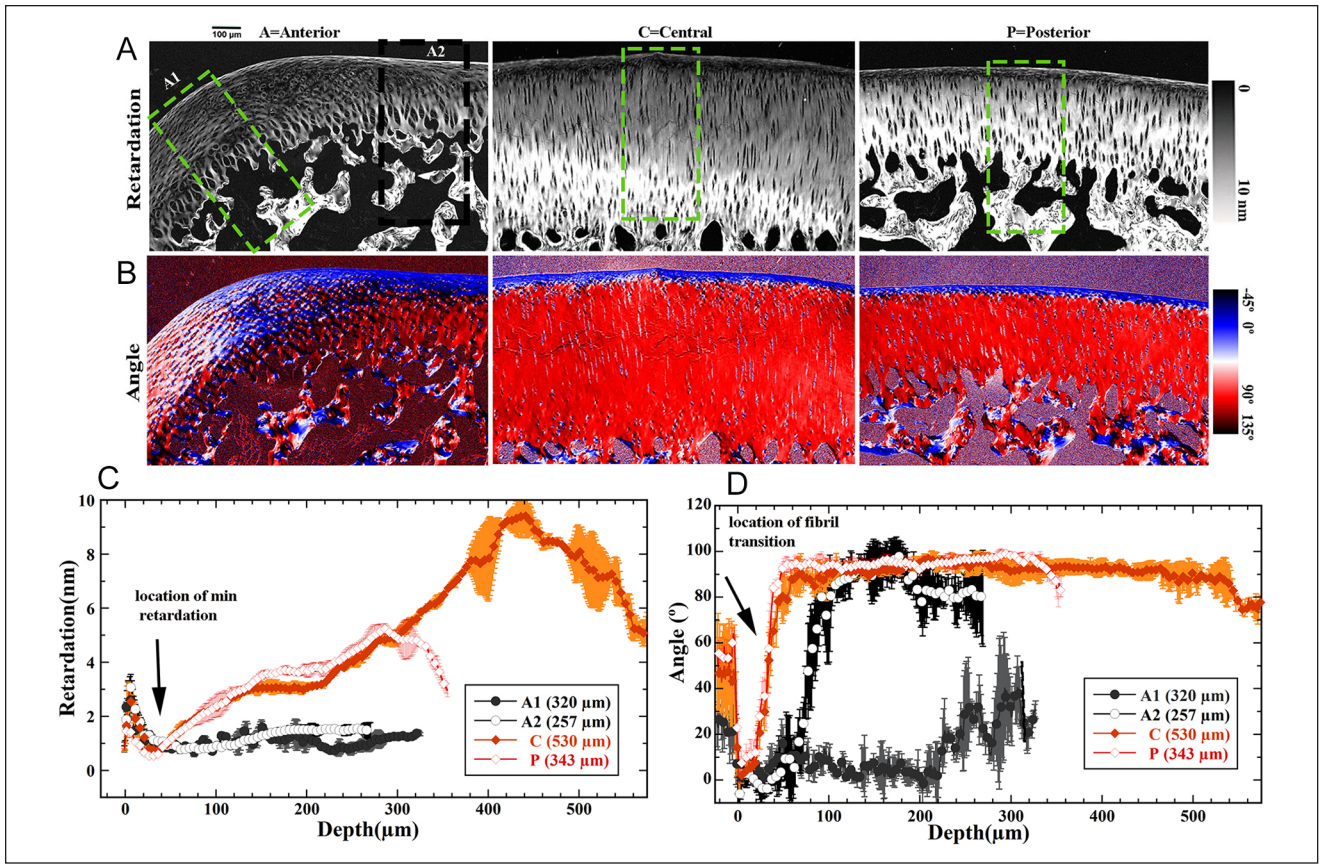

Figure 5. Three-dimensional quantitative PLM images of retardation (**A**) and angle (**B**), at 1 μm pixel resolution, from the cartilage specimens whose μMRI data were shown in **Figure 4**. The rectangular boxes in (**A**) show the locations where the depth-dependent profiles were calculated and are shown as the profiles in (**C**) and (**D**). The quantitative profiles for each location are the mean values (retardation and angle) obtained by averaging 3 histological sections from each specimen. The vertical error bars are the standard deviations in the averaging. The profiles are plotted for every fifth data point, but the standard deviations are shown for all data points. In the angle images, blue and red define a 90° orientational difference in collagen fibers. White represents 45° in the angle, which can be seen in large regions of the deep tissue in A1 (trochlear ridge). The thickness of the cartilage for each location is listed next to the figure legends in the black rectangular box. PLM = polarized light microscopy; μMRI = microscopic magnetic resonance imaging.

(toward TG side) of this specimen, which still has some similarity to the arched 3-zone structure, to the left end (toward TR side) of this specimen, where most of the deep cells become parallel with the articular surface, representing parallel architecture of collagen fibers at this location. Comparing the quantitative 1D retardation profiles of all locations (**Fig. 5C**), it is evident that the overall retardation values are lower for anterior than central and posterior specimens (weak mutual organization).

Third, among the 3 locations, the central cartilage was the thickest (550 μm), that is, about 50% thicker than the cartilage at both the anterior and posterior locations (250-300 μm). Although different in their total thickness, both central and posterior cartilage had approximately the same thickness in their SZs (10-15 μm) and an identical tissue retardance minimum (~30-35 μm below the articular surface, marked by the arrow in **Fig. 5C**).

Comparison Between μMRI and PLM

Figure 6 compares the T2 (0°) profiles from μMRI and the retardation profiles from PLM for the 4 topographical locations on the femoral condyle. In these quantitative profiles, the location of the minimum retardation indicates the location of the least ordered collagen fibrils in the tissue. By comparison, the location of the maximum T2 relaxation at 0° indicates the location of the least ordered water molecules in the tissue. Among the 4 locations, only the central cartilage (**Fig. 6C**) has a clearly matched correlation between the T2 peak and the retardation minimum, which is consistent with the previous observations in mature cartilage.[19] At the A2 location (**Fig. 6B**) and in posterior cartilage (**Fig. 6D**), the T2 peaks were less well-defined and the peak correlation between μMRI and PLM is lacking. The cartilage at the

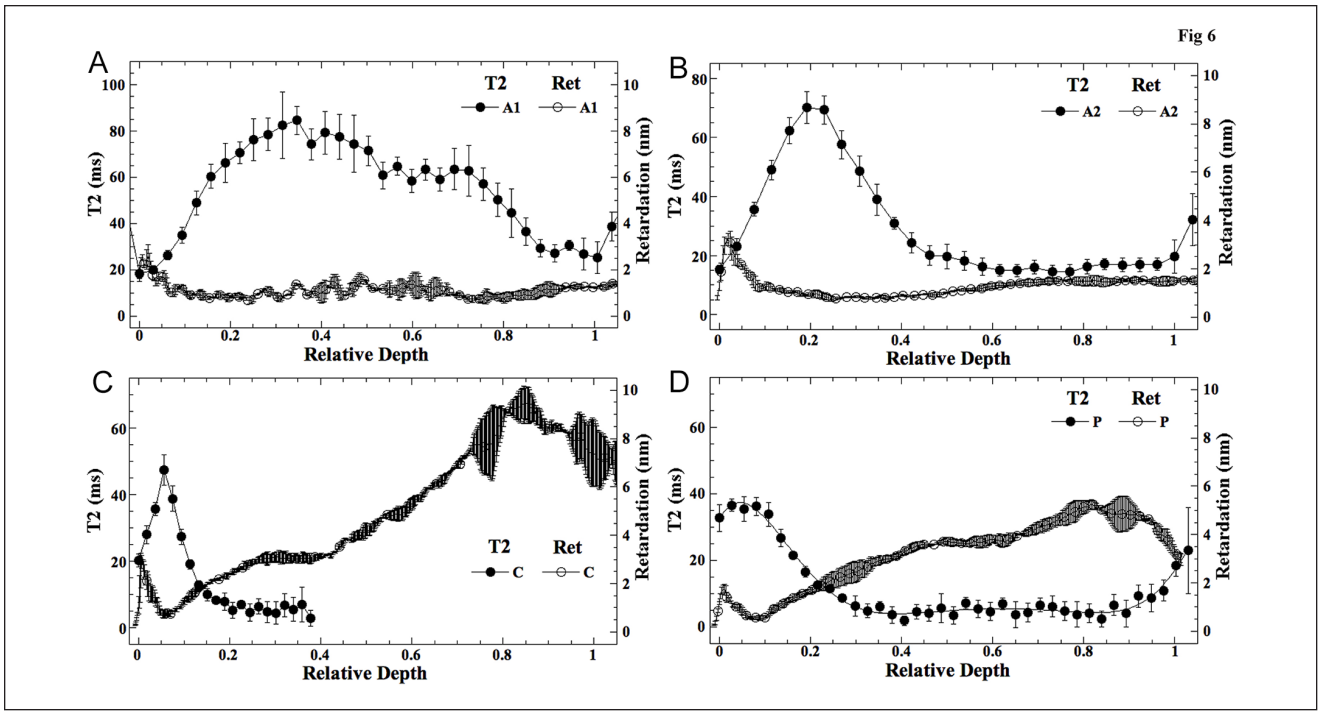

Figure 6. Comparison between the quantitative T2 profiles at 0° and the quantitative retardation profiles, at 4 different locations in femoral cartilage. 0 in the relative depth marks the articular surface, and 1 in the relative depth marks the cartilage–bone interface.

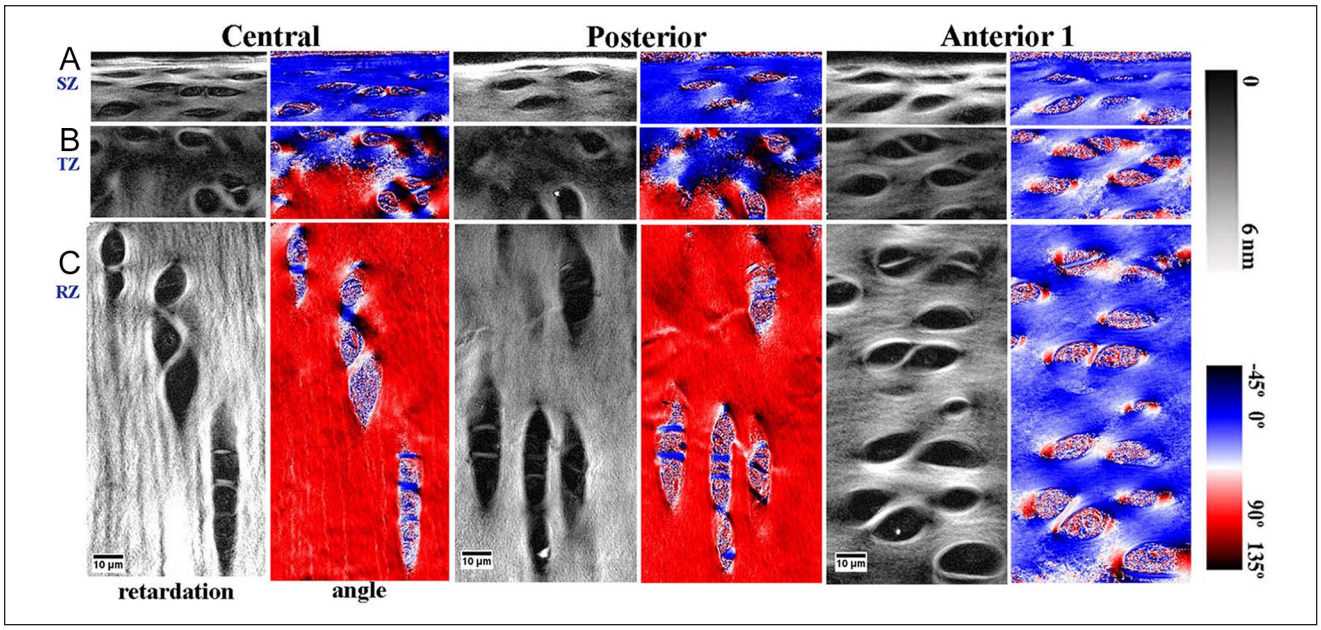

Figure 7. Quantitative PLM images of the 3 locations of tissue at 0.25 µm pixel resolution at different histological zones. (**A**) SZ images of all 3 locations at 5% of their relative thickness, (**B**) TZ images of all 3 locations at 10% of their relative thickness, and (**C**) RZ images at 40% of their relative thickness. PLM = polarized light microscopy; SZ = superficial zone; TZ = transitional zone; RZ = radial zone.

A1 location (**Fig. 6A**) does not have any recognizable feature that can be used to interpret the arched 3-zone fibril structure.

Territorial Matrix (40x Imaging)

Figure 7 shows the high-resolution quantitative angle and retardation images (40x objective, 0.25 µm/pixel) of the

cellular clusters at different depths from the same specimens used before in the 10x imaging (**Fig. 5**). Morphologically, one can use the quantitative retardation images to view the cellular structure, from which one can easily determine the zonal orientation of the cells and cellular clusters. In the SZ of all 3 sample locations, all cells had a spindle shape and oriented in parallel with the articular surface. In addition, the territorial and interterritorial fibers ran parallel to the articular surface (i.e., having blue in the angle images). In the central and posterior cartilage, the cellular clusters in TZ were more circular in shape, which implied the lack of a dominant orientation. Furthermore, the cellular clusters in RZ all oriented vertically—perpendicular to the articular surface, which can also be seen from red in the angle images. In contrast to the central and posterior cartilage, the cellular structures in RZ at the anterior location oriented approximately with the articular surface, which gives the anterior cartilage its lack of arched zonal structure. A higher cellular density can also be noted in the anterior cartilage—in particular, the anterior clusters were fatter than the central and posterior clusters, which implies larger aspect ratios of the oval shapes (aspect ratio = width/length).

Quantitatively, higher retardation values can be found in the proximity of cells and cellular clusters, which indicates the presence of a cocoon-shaped fibril structure surrounding each cell or each group of cells. The same cocoon-shaped fibril structure was also seen from the quantitative angle images when they were enlarged further, in which the angle values change in a cyclic manner, that is, the same color appears on the opposite side of the same cell or cellular cluster. As a collagen fiber has neither head nor tail, the same angle value appears on the opposite of any circular shape, which should have two 90° orientational differences, between blue and red, and between white and black. For the central and posterior cartilage, the background colors in the angle images, that is, the orientations of the territorial matrix in the tissue, had the expected 90° transition between the surface and deep cartilage, indicating an arched 3-zone structure. In contrast, the anterior cartilage (A1) had the same bluish color for all regions of the tissue, indicating an absence of a 3-zone structure.

Discussion

To the best of our knowledge, this is the first quantitative study of the topographical features of the femoral cartilage in a rabbit model by μMRI and PLM at microscopic resolutions. Compared with the use of larger animals, rabbits are small, inexpensive, and have more societal acceptance. As rabbit cartilage is thin, any depth-dependent examination requires high resolution in imaging. In recent years, the use of rabbit models in biomedical research has been gradually increasing.[9,17,20-23] Still, many features of the rabbit tissues, even in healthy control animals, have not been well characterized, which complicates the understanding of degenerative characteristics in tissue.

Topographical Structural Variations in Juvenile Joints

A better understanding of the developmental changes from juvenile tissue to mature tissue is critically important as younger populations can develop osteoarthritis several years after traumatic injuries. Studies of the juvenile canine humeral head and ovine distal metacarpus[24,25] have revealed a number of site-specific collagen structures, ranging from the arched 3-zone structure to complex multi-zone architecture, which can be seen on the same joint surface. Such site-specific collagen structures have also been found to be absent in mature canines.[19] These experimental observations support the notions that there are specific imaging features that are unique in juvenile joints, and that not all locations on the same juvenile joint develop into the 3-zone structure simultaneously. Probable explanation for these developmental differences at different locations on the same joint surface could be either variable growth rates, a pattern of the bone epiphysis, or exposure to different mechanical loading conditions at different anatomical sites of the same joint.[8,25-31]

This study showed that, for 3-month-old juvenile rabbits, the cartilage at the central and posterior locations along the femoral medial condyles had already developed into the classic 3-zone architecture, which is commonly seen in mature joints. In contrast, the cartilage at the anterior location, the TR of the patellofemoral region of the same joint, had no zonal architecture. This topographical difference could have 2 causes, namely, developmental and mechanical. The developmental cause is associated with the maturity of the cartilage, where distinct differences between the juvenile and mature cartilage in large animals have been noticed.[19,24] The mechanical cause is associated with the differences in the force patterns between the anterior location and the central and posterior locations. While the central and posterior cartilages are subject to large compressive loading, the anterior cartilage is subject to constant tangential motion with the patellar cartilage. Hence, the collagen fibers may adapt to the local mechanical environment.

As MRI T2 anisotropy is extremely sensitive to the dynamic environment of water molecules in biological tissue, it is expected that the fibril architecture and structural variations of the collagen network can be detected noninvasively and nondestructively by MRI if sufficient resolution can be achieved (as in μMRI). At the same time, this study also employed quantitative PLM protocols at higher optical resolution, which are uniquely sensitive to the mutual organization and overall orientation of the collagen matrix based on different physical principles. It has been shown previously that the retardance minimum below the articular

surface is closely associated with the geometric center of the TZ, which is represented by a maximum in quantitative T2 anisotropy of adult animals. The correlation between the 2 quantitative protocols can define the zonal architectures of the collagen network, from the classic 3-zone architecture to more complicated variations in juvenile tissues.

Intervention at an Early Stage

Understanding the differences between the juvenile and mature cartilage associated with the developmental stages and mechanical environments in individual animals (and humans) can contribute to better intervention of the cartilage degradation process at an early stage. The collagen network in cartilage is responsible for the structural stability of the tissue, which remodels continuously during growth and adolescence periods. After the skeletal maturation, the cartilage maintains a stable structure for the rest of the life span with only minor adaptations.[27] Studying the site and age-dependent mechanisms in the structural remodeling provides an opportunity to intervene/repair cartilage optimally at different ages when damage and degradation occur, which could prevent or postpone advanced stages of osteoarthritis. For example, sports-related injuries, common in young adults, can develop into osteoarthritis within a short time after the injury. Failure in cartilage repair could happen if the repair tissue does not fit the specific age and topographical dependent features of the damage location.

The development of arcade-like structures with age is an important and interesting phenomenon, the understanding of which would be beneficial to the design of superior materials and procedures as it would be more stable and better able to effectively handle the loading environment. Therapeutic improvements could potentially be implemented by identifying and investigating the localized physiological and mechanical factors involved at different sites on the same joint. For example, osteochondral allograft transplantations have been used to treat focal lesions in young and active patients. Considering the topographical variation in the fibril architecture can be helpful in dealing with site morbidity and also improve integration if the repair grafts can be designed to better match with neighboring/donor cartilage structurally.[32]

Experimental Notes

Structural changes in collagen fibril orientation are closely linked to compositional changes (PG and collagen content) in connective tissue. Due to technical limitations, we did not perform any histochemical analysis to determine any compositional difference of cartilage at different sites. In addition, as the development of the collagen network is a gradual process, we recognize the potential needs for more time points (i.e., different aged animals) to fully understand the developmental variations in the tissue architectures. The number of the μMRI sampling locations was 3, which were 4-6 mm apart from each other along the same small joint. It should also be noted that any topographical variations are highly dependent on the plane/location of histological cutting and the type of joint. Finally, any sample with curved surfaces (e.g., the anterior specimen in **Fig. 4**) cannot be set in any single experiment, with the entire surface at a particular orientation. This would also be true for any intact joint in human MRI. Any deviation from the nominal orientation would affect the T2 anisotropy, mainly through the geometric factor in the dipolar spin Hamiltonian.[12]

Note that, in physics, anisotropy is a descriptive term, which refers to the characteristic of a measurement that exhibits different values when measured along different directions. In MRI, the direction in the sample space is defined by the external magnetic field B0. A number of methods can be used to analyze the characteristic of T2 anisotropy. The first and original method analyzes directly the depth-dependent T2 profiles (as **Fig. 4C** of this study).[12] One can also combine these depth-dependent profiles into a 2D or peudo-3D anisotropy map, either without image interpolation (as **Fig. 5** in Xia *et al.*[16]) or with image smoothing/interpolation (as **Fig. 3** in Hänninen *et al.*[33]). Furthermore, one could calculate the percentage differences in these depth-dependent T2 profiles (as **Fig. 4** in Hänninen *et al.*[33]). In addition, if T2 anisotropy has been measured over a wide range of orientations in the 0° to 360° angular space, the relative contents of 2 orthogonal fibril bundles can be determined on a pixel-by-pixel basis (as **Fig. 7** and **Table 1** in Xia *et al.*[16]). In this study, our goal is to determine the structural variations at different anatomical locations of femoral cartilage in young rabbits. The direct comparisons among the μMRI and PLM profiles (**Fig. 6**) are sufficient to demonstrate clearly the nature of these location-specific anisotropies quantitatively.

Conclusion

μMRI and PLM imaging protocols were used to study the topographical variations among different locations on the medial femoral condyle of juvenile rabbits. Distinctly different characteristics of tissue properties were found in AC at different locations on femoral condyle in rabbits, likely related to the structural variations of different matrices in cartilage. As collagen organization plays a significant role in deciding the mechanical properties of tissue, our high-resolution imaging findings in the location-specific differences in knee joint's collagen organization can help to better understand localized mechanobiology of tissue. We believe our results could stimulate improvements in diverse fields, including developmental biology, tissue engineering, localized tissue degradation, design of more successful repair and replacement strategies, and diagnostic imaging.

Acknowledgments and Funding

Yang Xia is grateful to the National Institutes of Health (NIH) for an R01 grant (AR 69047). The authors thank Dr. Adam Lauver and Ms. Barbara Christian (Department of Pharmacology & Toxicology, Michigan State University) for providing the rabbit samples and Ms. Carol Searight (Department of Physics, Oakland University) for linguistic editing.

Declaration of Conflicting Interests

The author(s) declared no potential conflicts of interest with respect to the research, authorship, and/or publication of this article.

Ethical Approval

Ethical approval for the tissue study was waived by the Institutional Animal Care and Use Committee (IACUC) at Oakland University, because the specimens were the discarded tissue for an unrelated and approved experimental study.

ORCID iDs

Syeda Batool https://orcid.org/0000-0003-2491-1637
Yang Xia https://orcid.org/0000-0003-4653-1862

References

1. Calandruccio RA, Gilmer WSJ. Proliferation, regeneration, and repair of articular cartilage of immature animals. J Bone Joint Surg. 1962;44(3):431-55.
2. Li Y, Wei X, Zhou J, Wei L. The age-related changes in cartilage and osteoarthritis. Biomed Res Int. 2013;2013:916530.
3. Alhadlaq HA, Xia Y, Moody JB, Matyas JR. Detecting structural changes in early experimental osteoarthritis of tibial cartilage by microscopic magnetic resonance imaging and polarised light microscopy. Ann Rheum Dis. 2004;63(6):709-17.
4. Lee JH, Badar F, Matyas J, Qu X, Xia Y. Topographical variations in zonal properties of canine tibial articular cartilage due to early osteoarthritis: a study using 7-T magnetic resonance imaging at microscopic resolution. MAGMA. 2016;29(4):681-90.
5. Huang H, Skelly JD, Ayers DC, Song J. Age-dependent changes in the articular cartilage and subchondral bone of C57BL/6 mice after surgical destabilization of medial meniscus. Sci Rep. 2017;7(1):42294.
6. Teichtahl AJ, Wluka AE, Wijethilake P, Wang Y, Ghasem-Zadeh A, Cicuttini FM. Wolff's law in action: a mechanism for early knee osteoarthritis. Arthritis Res Ther. 2015;17(1):207.
7. Zambrano NZ, Montes GS, Shigihara KM, Sanchez EM, Junqueira LCU. Collagen arrangement in cartilages. Acta Anat (Basel). 1982;113(1):26-38.
8. Brommer H, Brama PAJ, Laasanen MS, Helminen HJ, van Weeren PR, Jurvelin JS. Functional adaptation of articular cartilage from birth to maturity under the influence of loading: a biomechanical analysis. Equine Vet J. 2005;37(2):148-54.
9. Julkunen P, Harjula T, Iivarinen J, Marjanen J, Seppänen K, Närh T, *et al*. Biomechanical, biochemical and structural correlations in immature and mature rabbit articular cartilage. Osteoarthritis Cartilage. 2009;17(12):1628-38.
10. Rieppo J, Hyttinen MM, Halmesmaki E, Ruotsalainen H, Vasara A, Kiviranta I, *et al*. Changes in spatial collagen content and collagen network architecture in porcine articular cartilage during growth and maturation. Osteoarthritis Cartilage. 2009;17(4):448-55.
11. Rubenstein JD, Kim JK, Morova-Protzner I, Stanchev PL, Henkelman RM. Effects of collagen orientation on MR imaging characteristics of bovine articular cartilage. Radiology. 1993;188(1):219-26.
12. Xia Y. Relaxation anisotropy in cartilage by NMR microscopy (μMRI) at 14-μm resolution. Magn Reson Med. 1998;39(6):941-9.
13. Xia Y, Moody JB, Burton-Wurster N, Lust G. Quantitative in situ correlation between microscopic MRI and polarized light microscopy studies of articular cartilage. Osteoarthritis Cartilage. 2001;9(5):393-406.
14. Lee JH, Xia Y. Quantitative zonal differentiation of articular cartilage by microscopic magnetic resonance imaging, polarized light microscopy, and Fourier-transform infrared imaging. Microsc Res Tech. 2013;76(6):625-32.
15. Alhadlaq H, Xia Y, Hansen FM, Les CM, Lust G. Morphological changes in articular cartilage due to static compression: polarized light microscopy study. Connect Tissue Res. 2007;48(2):76-84.
16. Xia Y, Moody JB, Alhadlaq H. Orientational dependence of T2 relaxation in articular cartilage: a microscopic MRI (μMRI) study. Magn Reson Med. 2002;48(3):460-9.
17. Batool S, Mahar R, Badar F, Tetmeyer A, Xia Y. Quantitative μMRI and PLM study of rabbit humeral and femoral head cartilage at sub-10 μm resolutions. J Orthop Res. 2020;38(5):1052-62.
18. Xia Y. Magic-angle effect in magnetic resonance imaging of articular cartilage: a review. Invest Radiol. 2000;35(10):602-21.
19. Xia Y, Moody JB, Alhadlaq H, Burton-Wurster N, Lust G. Characteristics of topographical heterogeneity of articular cartilage over the joint surface of a humeral head. Osteoarthritis Cartilage. 2002;10(5):370-80.
20. Frenkel SR, Bradica G, Brekke JH, Goldman SM, Ieska K, Issack P, *et al*. Regeneration of articular cartilage—evaluation of osteochondral defect repair in the rabbit using multiphasic implants. Osteoarthritis Cartilage. 2005;13(9):798-807.
21. Esteves PJ, Abrantes J, Baldauf H-M, BenMohamed L, Chen YX, Christensen N, *et al*. The wide utility of rabbits as models of human diseases. Exp Mol Med. 2018;50(5):1-10.
22. Wakitani S, Goto T, Young RG, Mansour JM, Goldberg VM, Caplan AI. Repair of large full-thickness articular cartilage defects with allograft articular chondrocytes embedded in a collagen gel. Tissue Eng. 1998;4(4):429-44.
23. Sah RL, Yang AS, Chen AC, Hant JJ, Halili RB, Yoshioka M, *et al*. Physical properties of rabbit articular cartilage after transection of the anterior cruciate ligament. J Orthop Res. 1997;15(2):197-203.
24. Xia Y, Moody JB, Alhadlaq H, Hu J. Imaging the physical and morphological properties of a multi-zone young articular cartilage at microscopic resolution. J Magn Reson Imaging. 2003;17(3):365-74.

25. van Turnhout MC, Schipper H, Engel B, Buist W, Kranenbarg S, van Leeuwen JL. Postnatal development of collagen structure in ovine articular cartilage. BMC Dev Biol. 2010;10(1):62.
26. Hudelmaier M, Glaser C, Hohe J, Englmeier KH, Reiser M, Putz R, *et al*. Age-related changes in the morphology and deformational behavior of knee joint cartilage. Arthritis Rheum. 2001;44(11):2556-61.
27. Heinemeier KM, Schjerling P, Heinemeier J, Møller MB, Krogsgaard MR, Grum-Schwensen T, *et al*. Radiocarbon dating reveals minimal collagen turnover in both healthy and osteoarthritic human cartilage. Sci Transl Med. 2016;8(346):346ra90.
28. Thonar EJ, Sweet MB. Maturation-related changes in proteoglycans of fetal articular cartilage. Arch Biochem Biophys. 1981;208(2):535-47.
29. Wong MWN, Qin L, Lee KM, Leung KS. Articular cartilage increases transition zone regeneration in bone-tendon junction healing. Clin Orthop Relat Res. 2009;467(4):1092-100.
30. Peters AE, Akhtar R, Comerford EJ, Bates KT. The effect of aging and osteoarthritis on the mechanical properties of cartilage and bone in the human knee joint. Sci Rep. 2018;8:5931.
31. Julkunen P, Iivarinen J, Brama PA, Arokoski J, Jurvelin JS, Helminen HJ. Maturation of collagen fibril network structure in tibial and femoral cartilage of rabbits. Osteoarthritis Cartilage. 2010;18(3):406-15.
32. Reddy S, Pedowitz DI, Parekh SG, Sennett BJ, Okereke E. The morbidity associated with osteochondral harvest from asymptomatic knees for the treatment of osteochondral lesions of the talus. Am J Sports Med. 2007;35(1):80-5.
33. Hänninen N, Rautiainen J, Rieppo L, Saarakkala S, Nissi MJ. Orientation anisotropy of quantitative MRI relaxation parameters in ordered tissue. Sci Rep. 2017;7:9606.